Dynamic transition from complete population transfer to self-induced transparency

Andreas Pusch, Joachim M. Hamm, and Ortwin Hess*

Blackett Laboratory, Department of Physics, Imperial College London, South Kensington Campus, London SW7 2AZ, United Kingdom

(Received 21 February 2012; published 5 April 2012)

We explore the connection between adiabatic rapid passage, a technique that allows for robust complete population transfer (CPT) in a resonant absorber, and self-induced transparency solitons. We employ the auxiliary differential equation finite-difference time-domain method to fully resolve the dynamics of femtosecond light pulses propagating through an absorbing two-level medium. Using the example of linearly chirped Gaussian pulses we find that the pulses achieving robust CPT for a single two-level system are also pulses that will transform into solitary waves when incident on a resonantly absorbing medium. At the entrance into the absorber strongly chirped, adiabatic pulses completely transfer the electronic population from the ground to the upper state. As the pulses suffer absorption they undergo a dynamic transition and quickly split into an off-resonant radiation part and one or several unchirped solitary pulses that may carry away some of the initially achieved population inversion. This spectral and temporal transformation process limits the spatial depths of the region of CPT in a dense absorber regardless of the initial pulse amplitude. We also show that the frequency-domain pulse area, defined as the spectral amplitude at the resonance frequency, allows for a better distinction between the regimes of 2π-pulse and 0π-pulse formation than time-domain measurements.

DOI: 10.1103/PhysRevA.85.043807 PACS number(s): 42.65.Tg, 42.50.Md, 82.53.−k, 05.45.Yv

I. INTRODUCTION

Studies of the resonant interaction of a light pulse with absorbing systems are usually concerned with either the induced electronic excitation or the propagation characteristics of the pulse. One of the most remarkable effects occurring when light pulses propagate through a resonant absorber is the possibility of a coherent cancellation of absorption by re-emission, known as self-induced transparency (SIT) [1–3]. In fact, assuming plane waves in the limit of a slowly varying envelope and unidirectional propagation, it has been proven that a sech-shaped 2π pulse constitutes a fundamental soliton of the nonlinear light-matter interaction [4]. If the plane-wave approximation is dropped, solitary propagation appears to be only possible in certain situations (e.g., in waveguides that allow for a laterally constant Rabi frequency [5,6] or as light bullets with a complicated lateral pulse shape [7]).

Considering the induced electronic excitation, the technique of adiabatic rapid passage (ARP) has been developed to achieve a complete population transfer (CPT) in multilevel systems (e.g., semiconductor quantum dots [8,9]) by illuminating them with strongly chirped, intense pulses [10–13]. As ARP is robust against small pulse detuning and variations in amplitude it allows the manipulation of the state of an electronic system with unmatched precision and has applications in fields as diverse as nuclear magnetic resonance [14], femtochemistry [15], single photon generation [16], and quantum computing [17]. In contrast to SIT, which is inherently nonlinear, ARP is commonly treated in linear approximation. This is possible for weak atomic (molecular) polarization in which case the feedback on the exciting light field can be ignored and only the Bloch equations need to be solved. Studies combining light propagation and population transfer have been performed theoretically, using the slowly varying envelope approximation (SVEA) and the rotating wave approximation (RWA), and experimentally [18,19]. There, it was found that strongly chirped pulses are subject to pulse reshaping and stimulated emission in dense ensembles of absorbers, which limits the efficiency of ARP.

In this article, we investigate the pulse reshaping process that constitutes a dynamic transition from complete population transfer to solitary propagation in the interaction between chirped pulses and a dense two-level medium. The creation of solitons out of moderately chirped pulses has previously been investigated for SIT [20,21] and also for Kerr solitons [22,23]. In Refs. [20,21] the number of solitons created asymptotically in dependence of chirp and pulse amplitude for different pulse shapes are calculated but the state of the two-level systems after passage of the pulses is not considered. Also, no results on the dynamics of the soliton generation could be obtained in those studies since static techniques such as conservation laws and the inverse scattering transform [24] were used.

Here, we use a rigorous model for plane-wave pulse propagation without employing RWA and SVEA, to study the interaction of linearly chirped sech-shaped few-cycle pulses with dipolar electronic transitions represented by quantum mechanical two-level systems. The approach taken is known as the auxiliary differential equation finite-difference time-domain (ADE-FDTD) approach [25,26] and integrates numerically the combined Maxwell-Bloch equations. We will explicitly show that and how plane-wave pulses that induce CPT in single atoms transform into solitons in dense ensembles of two-level systems, thereby limiting the efficiency of CPT in dense ensembles and at the same time enabling the creation of unchirped pulses out of arbitrarily (negatively or positively) chirped input pulses.

This article is organized as follows. Section II outlines the model equations and specifies the frequency-resolved optical gating (FROG) technique used for pulse analysis. In Sec. III we analyze the origin of CPT by comparing polarization and inversion of a single atom driven by light pulses that do or do not fulfill the conditions for ARP and thus identify the full time-domain signatures of adiabatic following. In addition,

*o.hess@imperial.ac.uk

we map and compare the regimes for soliton creation in dense ensembles and CPT for varying chirp and pulse amplitude and find that the adiabaticity condition resembles the pulse area theorem of SIT when it is formulated in frequency domain. Section IV explores the propagation of moderately chirped pulses in a dense ensemble of two-level systems. In this regime we find that the chirp is rapidly lost and that the pulses reshape into SIT solitons with intensity-dependent group velocity. Propagation of strongly chirped pulses well inside the CPT regime is investigated in Sec. V. Here, the pulses induce CPT for the first few wavelengths, undergo substantial absorption at the resonance frequency, and shed radiation while reshaping into solitary waves. The main findings of the present study are summarized in Sec. VI.

II. METHODS

The semiclassical equations governing the (nonlinear) propagation of electromagnetic fields through an atomic two-level system are the Maxwell-Bloch equations. For simplicity we here restrict ourselves to one-dimensional propagation and linear polarization of the electric field. The restriction to linear polarization does not lead to a loss of generality of the analysis [26]. The governing equations are then given by

$$\partial_t B = -\frac{E}{\partial z} \tag{1}$$

and

$$\partial_t(\epsilon_0 \epsilon E + P) = \frac{1}{\mu_0}\frac{\partial B}{\partial z}, \tag{2}$$

for the electric field $E(z,t)$ and the magnetic field $B(z,t)$. The polarization $P(z,t) = 2N\mu u(z,t)$ of the resonant absorber is calculated from

$$\begin{aligned} \partial_t u &= \omega v - \gamma_p u \quad \partial_t v = -\omega u - \frac{2E^{\mathrm{loc}}\mu}{\hbar} W - \gamma_p v \\ \partial_t W &= \frac{2\mu E^{\mathrm{loc}}}{\hbar} v - \gamma_r (W+1)/2, \end{aligned} \tag{3}$$

with relaxation γ_r of the inversion W and dephasing of the polarization γ_p. The local field effect is included for completeness, although its impact on the dynamics in the regime of short pulse durations is small [27]. The local field acting on the atom is given by [28]

$$E^{\mathrm{loc}}(z,t) = E(z,t) + P(z,t)/3\,. \tag{4}$$

We integrate Eqs. (1)–(4) using the ADE-FDTD method [29]. For accuracy, the Bloch equations are advanced in time with the fourth-order Runge-Kutta method using an interpolation of the electric field values at intermediate time steps [30]. Pulses are launched into the simulation domain using the total-field scattered-field technique [31] to inject a linearly chirped Gaussian pulse into the simulation domain at $z = 0$ with the time dependence of the electric field $E(t) = E_x(t)$ given by

$$E(t) = E_0 \cos\{[\omega_0 + \alpha(t-t_0)](t-t_0)\} \exp\left[\frac{t-t_0}{2\tau^2}\right]. \tag{5}$$

leading to a frequency domain field of

$$\tilde{E}(\omega) = \tilde{E}_0 \exp\left[-\frac{(\omega-\omega_0)^2}{2\Gamma^2} + i\alpha'\frac{(\omega-\omega_0)^2}{2}\right]. \tag{6}$$

The parameter α determines the magnitude of the linear temporal chirp, whereas α' is the linear spectral chirp and $\alpha\tau^2 = \alpha'/\Gamma^2$.

In time domain the pulse area θ_t is given by

$$\theta_t = \mu \int_{-\infty}^{\infty} dt\, E_0 \exp\left[\frac{t-t_0}{2\tau^2}\right], \tag{7}$$

whereas a frequency domain area can be defined by the electric field magnitude at the center frequency [32]

$$\theta_\omega = 2\mu\tilde{E}_0/(\Gamma\hbar). \tag{8}$$

Thus, the frequency domain area θ_ω and the time domain area θ_t are only equivalent if the chirp $\alpha = 0$ while $\alpha \neq 0$ results in $\theta_t > \theta_\omega$.

The pulse propagation is analyzed with the help of temporal pulse shapes, spectra, and FROG traces [33]. The polarization gate FROG technique employed here measures the following spectrogram

$$|E_g(\omega,\tau)|^2 \propto \left|\int_{-\infty}^{\infty} dt\, E_{\mathrm{signal}}(t,\tau) e^{-i\omega t}\right|^2, \tag{9}$$

with a signal field comprised of a product of electric field and its envelope as gate function

$$E_{\mathrm{signal}}(t,\tau) = E(t)g(t-\tau) = E(t)|E_{\mathrm{env}}(t-\tau)|^2\,. \tag{10}$$

III. PULSE AREA AND ADIABATICITY CONDITION

In this section we explore the full time-domain manifestations of adiabatic following as well as the connection between the pulse area of SIT theory and the adiabaticity condition on complete population transfer (CPT). Let us first look at the polarization and inversion dynamics during robust CPT via adiabatic rapid passage (ARP) in full time-domain. We consider a pulse with fixed frequency bandwidth Γ and different values of dimensionless chirp $\alpha\tau^2$ and frequency domain pulse area θ_ω. Figure 1 shows the excitation dynamics of a single coherent ($\gamma_p = \gamma_r = 0$) two-level system driven by an intense, chirped few-cycle pulse (FWHM of 5 cycles) for different values of chirp and frequency domain area. The complete rotation of the inversion W experienced for an unchirped 2π pulse gives way to a partially inverted system and finally, for sufficiently high chirp values, to CPT. For the unchirped pulse [Fig. 1(a)] the real part of the polarization (which couples back to the electric field) is always out of phase with the electric field and performs a phase jump of π at the point of maximum inversion. This phase jump leads to the re-emission that lies at the heart of self-induced transparency (SIT). For a moderate dimensionless chirp value of $\alpha\tau^2 = 2$ [Fig. 1(b)] the polarization has an indefinite phase relationship to the electric field. Therefore, the excitation only achieves a final inversion of $W \approx 0.5$ and a Rabi oscillation is still visible. When the pulse is strongly chirped [$\alpha\tau^2 = 5$, see Fig. 1(c)] the polarization is almost exactly in phase with the electric field. No sudden phase jump occurs and the polarization and electric field have almost identical pulse shapes, so that a final inversion

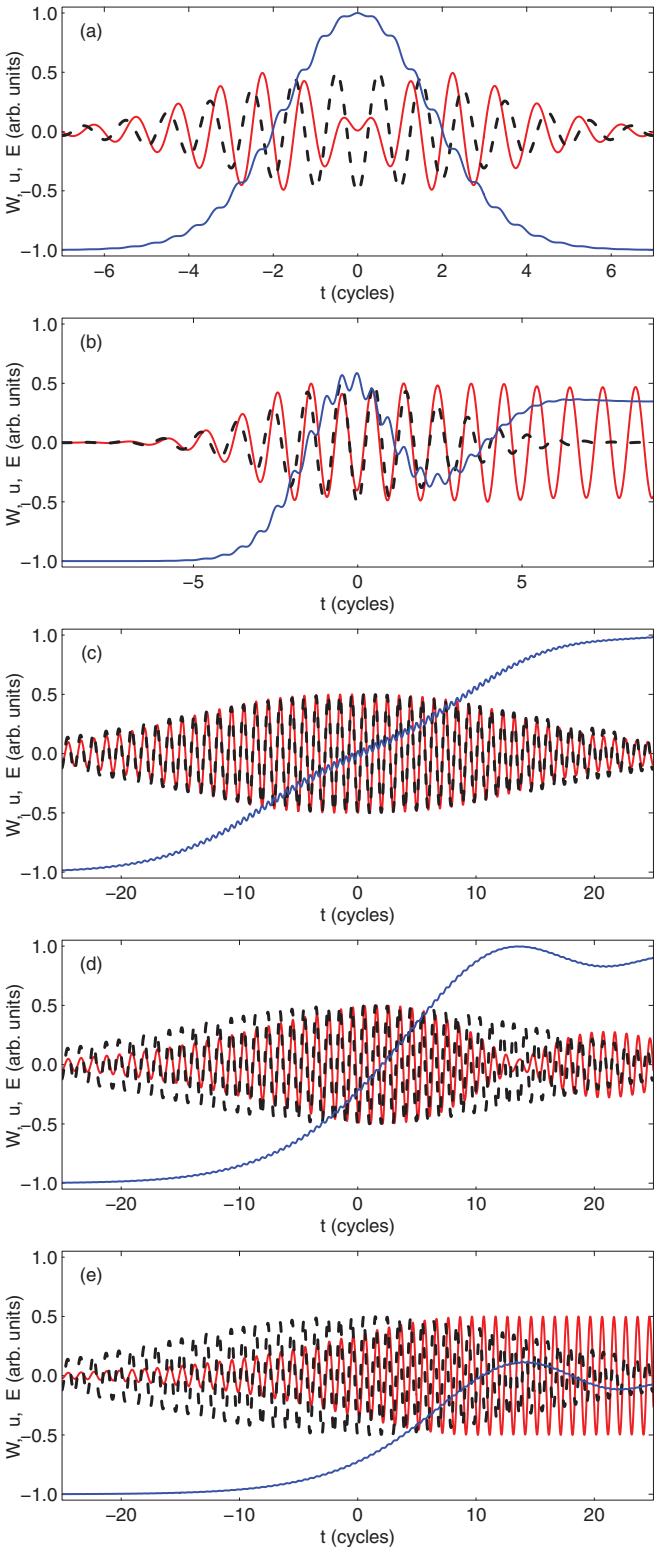

FIG. 1. (Color online) Evolution of a two-level system driven by a pulse with different values of frequency domain pulse area and chirp (a) $\alpha\tau^2 = 0$, $\theta_\omega = 2\pi$, (b) $\alpha\tau^2 = 2$, $\theta_\omega = 2\pi$, (c) $\alpha\tau^2 = 5$, $\theta_\omega = 2\pi$, (d) $\alpha\tau^2 = 5$, $\theta_\omega = \pi$, and (e) $\alpha\tau^2 = 5$, $\theta_\omega = \pi/2$. The inversion W is given by the blue (dark gray) solid line, the real part of the polarization by the red (light gray) solid line and the electric field by the black dashed line.

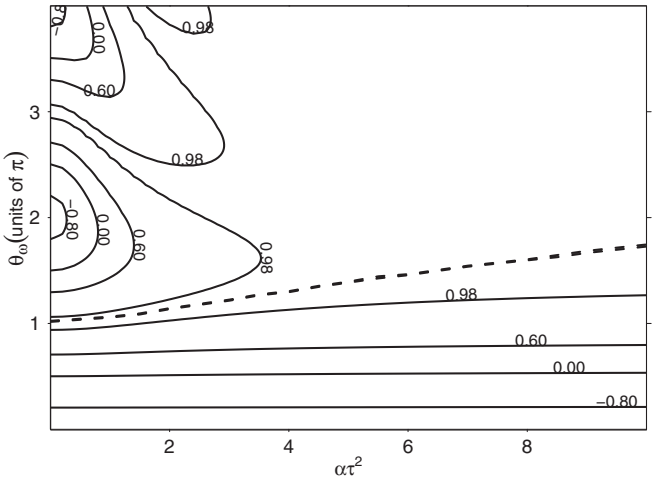

FIG. 2. Contour plot of the final inversion W of a single two-level system after excitation by a pulse with area θ and dimensionless chirp $\alpha\tau^2$. Above the dashed line, 2π pulses are created in a dense ensemble of two-level systems. Note, that the contour plots in the negative chirp regime are an exact mirror image of the positive chirp regime (compare Fig. 4 of Ref. [13]).

of $W \approx 1$ can be reached without visible Rabi oscillations. Thus, we conclude that adiabatic following manifests itself in full time domain as a polarization almost in phase with the electric field and following its pulse shape. Reducing the pulse area of the strongly chirped pulse to a value of $\theta_\omega = \pi$ [see Fig. 1(d)] introduces an oscillatory tail in the population inversion, leading to an incomplete final inversion, which is occasioned by an imperfect following of the polarization for late times. These imperfections increase for lower pulse areas [see Fig. 1(e)] such that the final inversion is further reduced.

The regime of robust CPT is shown in Fig. 2, containing a contour plot of the inversion reached in a single atom when it is excited by a Gaussian pulse of area θ_ω and dimensionless linear chirp $\alpha\tau^2$. The spectral chirp required to achieve ARP is best expressed in terms of a dimensionless linear chirp $|\alpha|\tau^2 = |\alpha'|/\Gamma^2 \gg 1$. The necessary pulse amplitude is given by $\theta_\omega \gg \pi$ [13], which is a reformulation of the adiabaticity condition in terms of pulse area.

In addition to the impact of the exciting light pulses on a single atom we also studied the propagation behavior of the light pulse in a dense ensemble of two-level systems. Here, we assumed a dephasing rate of $0.001 f_0$, a two-level density of $N = 10^6\lambda^{-3}$, and a dipole length of $d = 10^{-4}\lambda$. The dashed line in Fig. 2 denotes the approximate critical initial pulse area needed for a 2π pulse to be created in the numerical simulations. Note that a 2π pulse in the presence of dephasing and backscattering does not strictly constitute a soliton since it eventually decays and that it is therefore difficult to distinguish a 2π pulse from background radiation close to the critical area. It can be seen that for high chirp values a 2π pulse is only created if the pulse is well inside the regime of complete population transfer. The comparison between the conditions for ARP and the condition for soliton creation thus reveals the deep connection between the phenomena of SIT solitons and ARP. Indeed, Fig. 2 shows that pulses, which achieve

robust CPT in single two-level systems reshape into solitary waves when propagating through a dense ensemble of two-level systems.

In the following section we investigate the dynamical reshaping process of pulses in resonant absorbers. As a first step, we study moderately chirped pulses with a chirp value of $\alpha\tau^2 = 1$, insufficient for robust CPT via ARP (Sec. IV). For these parameters we see the creation of unchirped solitary waves and radiation and are able to illustrate the difference between frequency-domain pulse area and time-domain pulse area for chirped pulses. The dynamics of strongly chirped pulses with $\alpha\tau^2 \gg 1$ propagating through a dense ensemble of two-level systems is investigated in Sec. V. Here, the dynamic transition from CPT to solitary propagation of one or several solitary waves and its limiting impact on the achievable population inversion becomes evident.

IV. RESHAPING OF MODERATELY CHIRPED PULSES

Moderately chirped pulses with a dimensionless chirp on the order of $\alpha\tau^2 \approx 1$ are neither capable of robust CPT nor do they achieve a full Rabi oscillation of the Bloch vector as can be seen from Fig. 2. Therefore, for such pulses propagating through a dense absorber some initial absorption is expected as well as a reshaping into a solitary wave if $\theta_\omega > 1.1\pi$. As we want to study differences in group velocities, which are more pronounced the denser the absorber and the longer the pulses we assume a dense ensemble of two-level systems with $N = 10^7\lambda^{-3}$, a dephasing rate of $\omega_0/1000$, and Gaussian pulses of 12 cycles duration (FWHM).

Pulses that propagate through the system first lose amplitude but then stay stable apart from the decay associated with dephasing and backscattering. Figure 3 shows the FROG traces of initial pulses and pulses after propagation through the ensemble of two-level systems. The chirp disappears in propagation for both initially negatively or positively chirped pulses. If the amplitude of the initial pulse corresponds to a frequency domain area $\theta_\omega = 2\pi$ [see Figs. 3(c) and 3(d)] the pulses narrow in time domain and narrow only slightly in frequency domain due to some initial absorption. If, however, the amplitude of the initial pulse is smaller [see Figs. 3(e) and 3(f)], so that it corresponds to a time domain area of 2π the temporally broadening pulses narrow significantly in frequency domain.

These last observations can be appreciated more clearly by comparing the spectra of the pulses, shown in Fig. 4(a). Firstly, the narrowing of the pulses in frequency domain that the FROG traces already suggested is clearly visible in the spectra together with a reshaping of the pulse from a Gaussian pulse to the sech-shaped pulse typical of a soliton. Pulses with less initial amplitude are narrower in frequency domain and therefore broader in time domain as expected from the pulse area theorem. Furthermore, all pulses have the same amplitude at the resonance frequency, confirming the usefulness of the frequency domain formulation of the area theorem. The radiation part of the final pulses introduces the oscillations at the flanks of the spectrum.

Figure 4(b) shows the temporal pulse envelopes after propagation for the different cases depicted in Fig. 4(a). As SIT theory predicts the solitary waves created from the

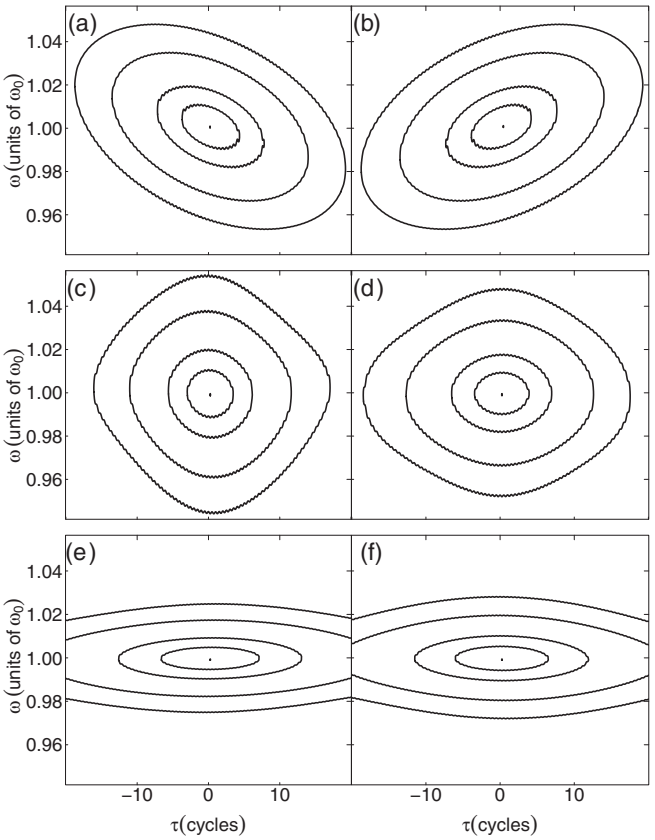

FIG. 3. FROG plots calculated from Eq. (10) for positive (left) and negative (right) initial chirp of $\alpha\tau^2 = 1$. (a) and (b) show the initial pulses, (c) and (d) the final FROG traces of pulses with initial frequency domain area of 2π and (e) and (f) the final FROG traces of pulses with initial time domain area of 2π. The contour lines indicate 80%, 60%, 40%, and 20% of the maximum values respectively.

less intense initial pulses experience a longer delay, are less intense, and are wider in the temporal domain. Secondly, a comparison between negatively and positively chirped pulses reveals that the negatively chirped pulses have a slightly longer delay. Nevertheless, the pulse with time domain area 2π and negative chirp is slightly more intense than its positively chirped counterpart, an unexpected combination that may be caused by a slower reshaping and stimulated emission process for positively chirped pulses.

V. PROPAGATION OF STRONGLY CHIRPED PULSES: DYNAMICAL TRANSITION FROM COMPLETE POPULATION TRANSFER TO SELF-INDUCED TRANSPARENCY

In this section we investigate the dynamical transition from CPT to SIT, using the same parameters for the two-level system as in the previous section. The transform-limited pulse length is kept at 12 cycles FWHM but a greater chirp is applied, so that we are well inside the regime of robust CPT. Pulse A has a chirp of $\alpha\tau^2 = 5$, corresponding to the single atom response of Fig. 1(c) and a frequency domain pulse area $\theta_\omega = 3\pi$; pulse B is characterized by $\alpha\tau^2 = 5$ and $\theta_\omega = 4\pi$; and pulse C by $\alpha\tau^2 = 10$ and $\theta_\omega = 3\pi$.

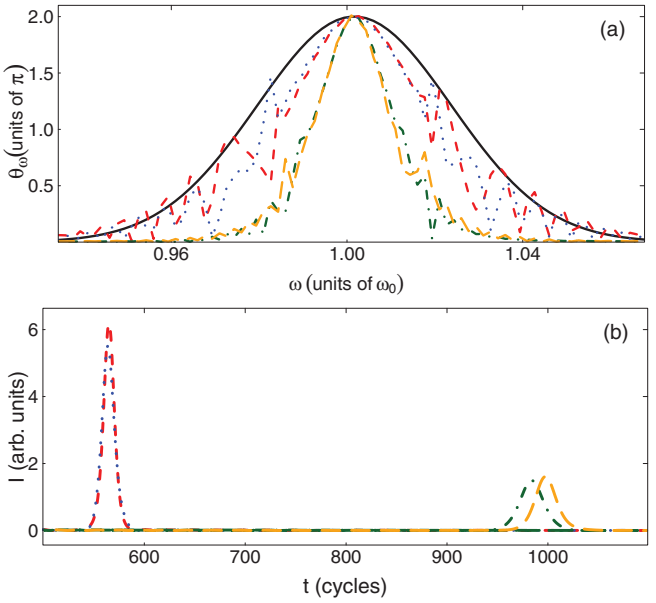

FIG. 4. (Color online) (a) Spectra of initial pulse with $\theta_\omega = 2\pi$, $\alpha\tau^2 = 1$, and $\tau_0 = 12$ cycles (solid black line), compared to spectra of final pulses after propagation for $\theta_\omega = 2\pi$ and $\alpha\tau^2 = 1$ (short-dashed red line) or $\alpha\tau^2 = -1$ (dotted blue line); and for $\theta_t = 2\pi$ and $\alpha\tau^2 = 1$ (dash-dotted dark green line) or $\alpha\tau^2 = -1$ (long-dashed orange line). (b) Intensity envelopes after propagation for the final pulses.

In Fig. 5 we present the spatiotemporal dynamics of the inversion of the dense ensemble of two-level systems excited by pulses A (a), B (b), and C (c). We can see the transition from CPT to transparency for all three cases. Pulse A evolves into two solitary waves that each achieve a complete rotation of the Bloch vector (i.e., they are 2π pulses). At a later point in time (not inside range of graphs), another weak pulse develops from the inverted two-level system and eventually gets absorbed again due to the dephasing in the atomic system. By this mechanism some of the population inversion achieved at the entrance into the medium is stripped away. Pulse B, which has an increased pulse area of 4π, initially excites population across a larger region at the entrance into the medium but another spawned solitary wave later distributes this inversion deeper into the ensemble of two-level systems. Also, two fast pulses are created instead of one. When the chirp is increased (pulse C) the region of effectively achieved CPT in the long time limit does not increase significantly. Again fast solitary waves, slow solitary waves, and radiation carry most of the excitation energy away.

In order to understand the process of formation of solitary waves out of CPT we can study the electric field spectra at different spatial points along the absorbing medium. Figure 6 compares, for pulse A, the input spectrum with spectra taken at $z = 4\lambda$ and $z = 8\lambda$ inside the absorbing medium. For $z = 4\lambda$ and for $z = 8\lambda$ most of the spectral amplitude is decreased, an indication that absorption has taken place. At $z = 4\lambda$ absorption has eaten away most of the pulse amplitude close to the resonance frequency. The peak at the resonance frequency can be understood as the late, slow solitary wave that builds in the top left corner of Fig. 5(a). At $z = 8\lambda$ the frequencies close to resonance are partially restored at the expense of frequencies

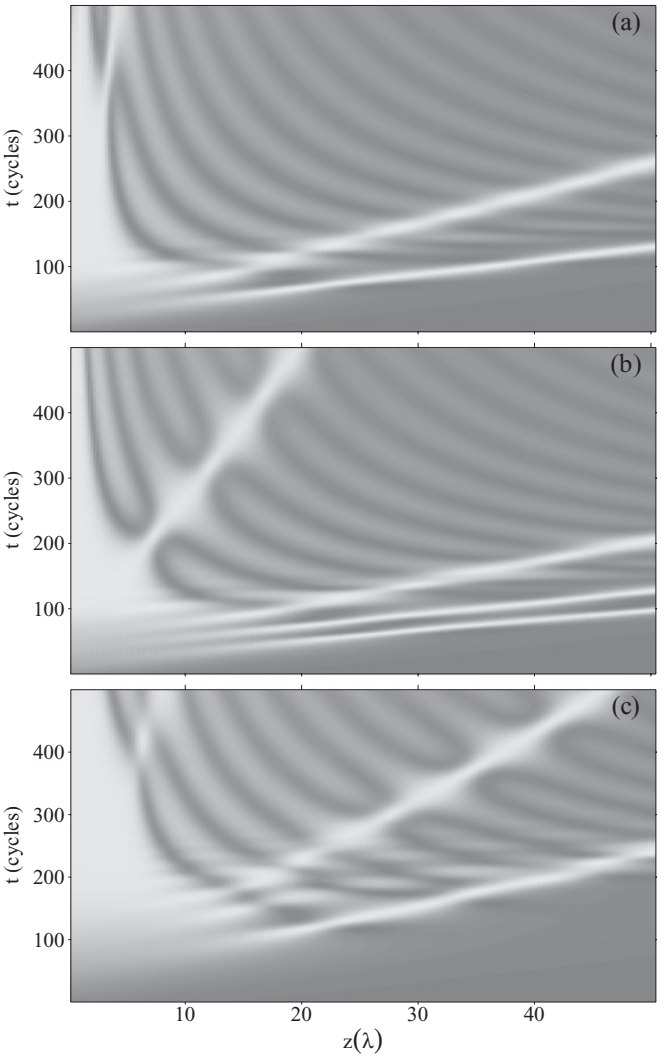

FIG. 5. Inversion W (black: $W = -1$, white: $W = 1$) plotted over time and propagation distance for initial pulses with $\theta_\omega = 3\pi$ and $\alpha\tau^2 = 5$ (a), $\theta_\omega = 4\pi$ and $\alpha\tau^2 = 5$ (b), and $\theta_\omega = 3\pi$ and $\alpha\tau^2 = 10$ (c).

further away from resonance, an indication of the formation of a solitary wave that is spectrally narrower than the initial

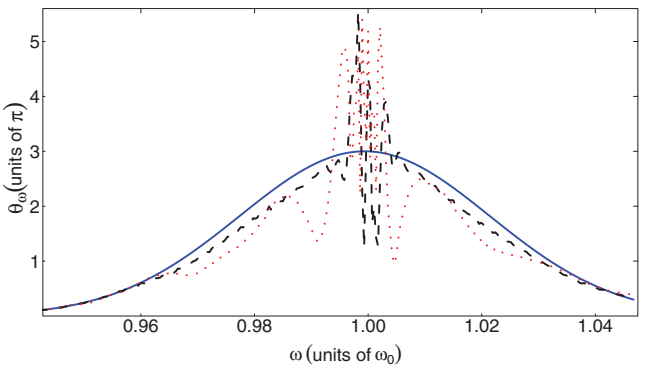

FIG. 6. (Color online) Initial pulse spectrum (solid blue line) compared to pulse spectra taken at $z = 4\lambda$ (dashed black line) and $z = 8\lambda$ (dotted red line) for pulse A [Fig. 5(a)].

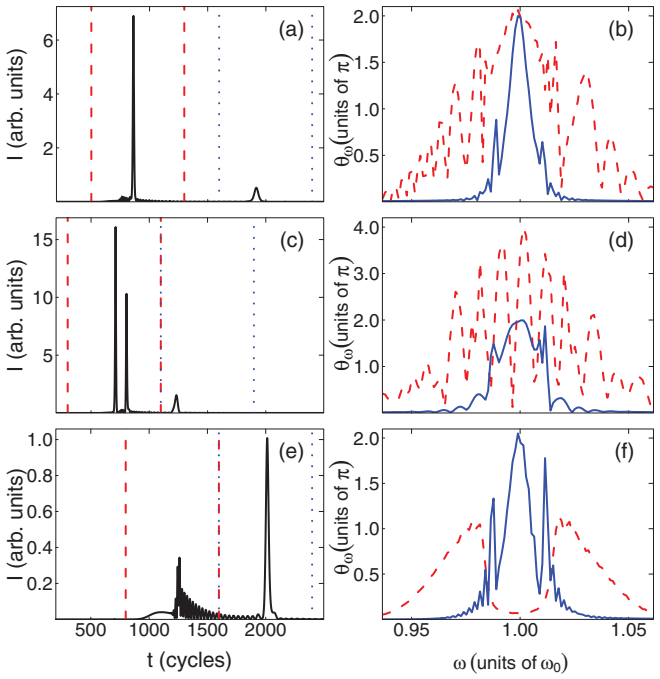

FIG. 7. (Color online) Pulse envelopes and spectra for pulses that propagated 200λ through the absorber. Initial pulse area and dimensionless chirp are: (a) and (b) $\theta_\omega = 3\pi$ and $\alpha\tau^2 = 5$, (c) and (d) $\theta_\omega = 4\pi$ and $\alpha\tau^2 = 5$, (e) and (f) $\theta_\omega = 3\pi$ and $\alpha\tau^2 = 10$. The spectra are taken in the time windows indicated by the dashed red line on the right for the dashed red line on the left and by the dotted blue line on the right for the solid blue line on the left. Note that the intensity scales are not uniform across the graphs.

pulse. In fact, at $z = 8\lambda$ CPT is not observed anymore, as the exciting pulse has already split into soliton and radiation parts. Radiation is mostly responsible for the strong oscillations in the spectrum. A narrow soliton peak on top of the broader soliton peak of the fast 2π pulse is the consequence of a second, slower solitary wave. These results clearly indicate that the formation of 2π pulses out of strongly chirped pulses involves a complex interplay between absorption, dispersion, and nonlinear processes that dynamically alter the frequency content of the pulse over very short length scales.

In Fig. 7 we show pulse envelopes and spectra at the exit of the medium (i.e., at a distance where the reshaping of the pulses has been achieved). Because of the long propagation distance, the slow solitary waves have accumulated a considerable delay and can be clearly separated. The spectra are taken in two time windows, the first of which contains the fast propagating radiation part and intense solitary waves whereas the second window contains only the slow propagating solitary wave. These results illustrate some of the fundamental aspects of SIT and clearly show the solitary wave character of the propagation. For pulse A [Figs. 7(a) and 7(b)], two solitary waves arrive, one of which is fast, intense, very short, and has a broad spectrum (again, the oscillations in the spectrum are caused by radiation). In contrast, the slower pulse is less intense, longer in duration, and with a narrower spectrum. The spectral amplitude at the resonance frequency of both pulses corresponds to $\theta_\omega = 2\pi$. Increasing the initial amplitude to $\theta_\omega = 4\pi$ (pulse B) leads to the creation of an additional pulse [as already observed in the inversion map (Fig. 5)] that also propagates very fast, so that the first two pulses cannot be separated in the spectrum [see Figs. 7(c) and 7(d)]. Because of their close proximity the pulses interact via the absorbing medium and are not independent solitary waves. In the spectrum the interaction between the pulses manifests itself as oscillations that reach up to 4π. Exactly at resonance it only reaches 2π, again illustrating that these two pulses cannot be seen as independent entities, while the slowly propagating pulse constitutes another, well separated 2π pulse.

The last row of Fig. 7 shows pulse C with an even higher chirp of $\alpha\tau^2 = 10$. Here, only one soliton is created out of the initial pulse of area $\theta_\omega = 3\pi$. Although the initial electric field could be confused with a solitary wave in time domain, the spectra clearly show that only the second part is a 2π pulse with a 2π amplitude at the central frequency. The first strong electric field pulse registered in time domain is completely off-resonant, containing merely radiation. Figure 7, in particular panels 7(e) and 7(f), reveal the importance of measuring the pulse spectra in order to determine the nature of a pulse propagating through resonant absorbers. The spectral amplitude at resonance gives a simple criterion for the experimental distinction between a 2π pulse

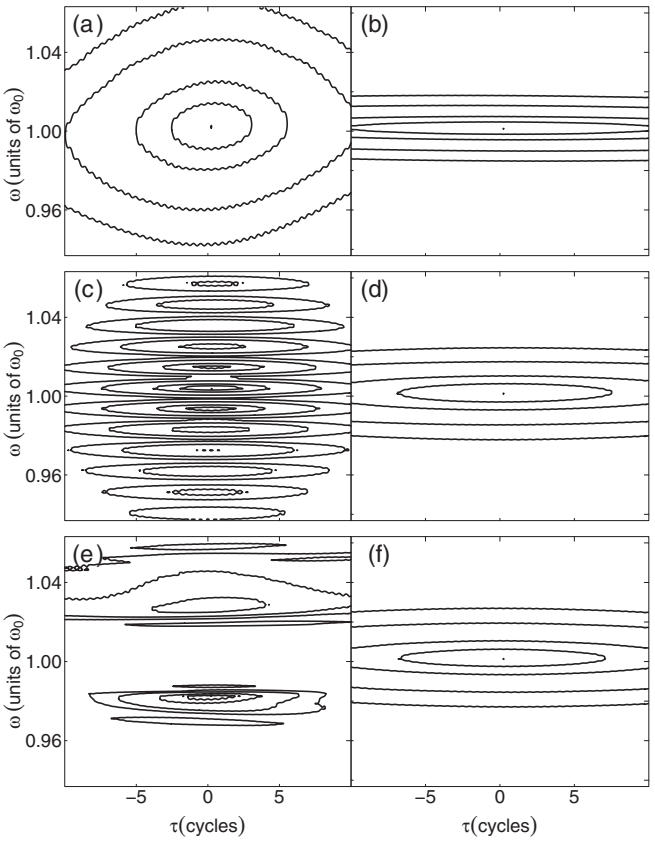

FIG. 8. (a) and (b) polarization gate FROG traces corresponding to Fig. 7(b); (c) and (d) corresponding to Fig. 7(d); and (e) and (f) corresponding to Fig. 7(f). The FROG traces on the left [(a), (c), and (e)] are taken for the earlier time windows and the traces on the right [(b), (d), and (f)] are taken for the later time windows, as marked by dashed (dotted) lines in Fig. 7. The contour lines indicate 80%, 60%, 40%, and 20% of the maximum values respectively.

and an off-resonant 0π pulse. The measured temporal pulse shape without phase information is not sufficient to distinguish between off-resonant 0π pulses and resonant 2π pulses.

Polarization gate FROG traces of pulses A–C after propagation have been taken in the time windows shown on the right of Fig. 7 and are depicted in Fig. 8. The fast pulses are depicted on the right; the slow, delayed solitary waves on the left. For both fast and slow pulses the chirp has clearly disappeared as the FROG traces are symmetric with regards to $\tau = 0$. However, for the fast pulses corresponding to Figs. 7(d) and 7(f) the complicated spectral structure is reproduced in their FROG traces. The FROG traces on the right, in contrast, largely correspond to simple, sech-shaped, transform-limited pulses with different broadening, in other words they are FROG traces of the fundamental 2π pulses of SIT theory. Hence, the FROG traces illustrate most clearly the transformation of strongly chirped pulses after propagation through a resonant absorber.

VI. CONCLUSION

In this article we investigated the dynamic transition from complete population transfer (CPT) via adiabatic rapid passage (ARP) to self-induced transparency (SIT) by numerically integrating the Maxwell-Bloch equations for chirped pulses incident on a resonantly absorbing medium. For moderate initial chirp the pulses quickly reshape into solitary waves, suffering weak absorption at entrance into the medium. In contrast, strongly chirped pulses suffer substantial absorption while initially achieving CPT but they also form into solitary waves during propagation. The spectral amplitude at resonance recovers and unchirped solitons emerge as clearly illustrated by the symmetry of the FROG traces with regard to positive and negative delay. Because of the reshaping process and stimulated emission from regions of inverted population into additional solitary waves, CPT is not achievable via ARP across dense ensembles. Consequently, increases in chirp or pulse area do not cause the deposition of more inversion in the system but rather lead to more energy being converted into solitary waves.

Having studied chirped pulse propagation using the time-domain and frequency-domain pulse area theorem we finally remark that neither theorem is able to correctly predict the number of created solitons from chirped pulses. A frequency-domain definition, however, proves to be more useful since it allows to more clearly distinguish between 2π pulses and 0π pulses [32]. The results presented show the limits of adiabatic techniques for population transfer and highlight the importance of combining time-domain and frequency-domain approaches when investigating resonant pulse propagation.

ACKNOWLEDGMENTS

Support by the Leverhulme trust is gratefully acknowledged.

[1] S. L. McCall and E. L. Hahn, Phys. Rev. Lett. **18**, 908 (1967).
[2] S. L. McCall and E. L. Hahn, Phys. Rev. **183**, 457 (1969).
[3] A. I. Maimistov, A. M. Basharov, S. O. Elyutin, and Y. M. Sklyarov, Phys. Rep. **191**, 1 (1990).
[4] R. K. Bullough, P. J. Caudrey, J. C. Eilbeck, and J. D. Gibbon, Opt. Quantum Electron. **6**, 121 (1974).
[5] U. Langbein, F. Lederer, and H. E. Ponath, Opt. Quantum Electron. **16**, 251 (1984).
[6] A. Pusch, J. M. Hamm, and O. Hess, Phys. Rev. A **84**, 023827 (2011).
[7] M. Blaauboer, B. A. Malomed, and G. Kurizki, Phys. Rev. Lett. **84**, 1906 (2000).
[8] Y. Wu, I. M. Piper, M. Ediger, P. Brereton, E. R. Schmidgall, P. R. Eastham, M. Hugues, M. Hopkinson, and R. T. Phillips, Phys. Rev. Lett. **106**, 067401 (2011).
[9] C.-M. Simon, T. Belhadj, B. Chatel, T. Amand, P. Renucci, A. Lemaitre, O. Krebs, P. A. Dalgarno, R. J. Warburton, X. Marie, and B. Urbaszek, Phys. Rev. Lett. **106**, 166801 (2011).
[10] W. S. Warren, H. Rabitz, and M. Dahleh, Science **259**, 1581 (1993).
[11] J. S. Melinger, S. R. Gandhi, A. Hariharan, D. Goswami, and W. S. Warren, J. Chem. Phys. **101**, 6439 (1994).
[12] N. V. Vitanov, T. Halfmann, B. W. Shore, and K. Bergmann, Annu. Rev. Phys. Chem. **52**, 763 (2001).
[13] V. S. Malinovsky and J. L. Krause, Eur. Phys. J. D **14**, 147 (2001).
[14] W. Warren, Science **242**, 878 (1988).
[15] A. Assion, T. Baumert, M. Bergt, T. Brixner, B. Kiefer, V. Seyfried, M. Strehle, and G. Gerber, Science **282**, 919 (1998).
[16] C. Brunel, B. Lounis, P. Tamarat, and M. Orrit, Phys. Rev. Lett. **83**, 2722 (1999).
[17] D. Goswami, Int. J. Quantum Inf. **5**, 179 (2007).
[18] M. R. Fetterman, J. C. Davis, D. Goswami, W. Yang, and W. S. Warren, Phys. Rev. Lett. **82**, 3984 (1999).
[19] J. C. Davis, M. R. Fetterman, W. S. Warren, and D. Goswami, J. Chem. Phys. **128**, 154312 (2008).
[20] R. T. Deck and G. L. Lamb, Phys. Rev. A **12**, 1503 (1975).
[21] L. V. Hmurcik and D. J. Kaup, J. Opt. Soc. Am. **69**, 597 (1979).
[22] K. Blow and D. Wood, Opt. Commun. **58**, 349 (1986).
[23] M. Böhm and F. Mitschke, Appl. Phys. B **86**, 407 (2007).
[24] V. E. Zakharov and A. B. Shabat, Funct. Anal. Appl. **8**, 226 (1974).
[25] R. W. Ziolkowski, J. M. Arnold, and D. M. Gogny, Phys. Rev. A **52**, 3082 (1995).
[26] A. Pusch, J. M. Hamm, and O. Hess, Phys. Rev. A **82**, 023805 (2010).
[27] D. V. Novitsky, Phys. Rev. A **82**, 015802 (2010).
[28] C. M. Bowden and J. P. Dowling, Phys. Rev. A **47**, 1247 (1993).
[29] Y. Niu, K. Xia, N. Cui, S. Gong, and R. Li, Phys. Rev. A **78**, 063835 (2008).
[30] Y. Loiko and C. Serrat, Phys. Rev. A **73**, 063809 (2006).
[31] A. Taflove and S. C. Hagness, *Computational Electrodynamics: The Finite-Difference Time-Domain Method*, 3rd ed. (Artech House, Norwood, Massachusetts, 2005).
[32] F. A. Hopf and M. O. Scully, Phys. Rev. B **1**, 50 (1970).
[33] R. Trebino, K. W. DeLong, D. N. Fittinghoff, J. N. Sweetser, M. A. Krumbugel, B. A. Richman, and D. J. Kane, Rev. Sci. Instrum. **68**, 3277 (1997).